Citation: Molecular Therapy—Nucleic Acids (2016) 5, e342; doi:10.1038/mtna.2016.55
Official journal of the American Society of Gene & Cell Therapy
www.nature.com/mtna

Silencing Myostatin Using Cholesterol-conjugated siRNAs Induces Muscle Growth

Tayeba Khan[1], Hans Weber[2], Jillian DiMuzio[1], Andrea Matter[1], Belma Dogdas[3], Tosha Shah[3], Anil Thankappan[1], Jyoti Disa[4], Vasant Jadhav[1], Laura Lubbers[2], Laura Sepp-Lorenzino[1], Walter R Strapps[1] and Marija Tadin-Strapps[4]

Short interfering RNAs (siRNAs) are a valuable tool for gene silencing with applications in both target validation and therapeutics. Many advances have recently been made to improve potency and specificity, and reduce toxicity and immunostimulation. However, siRNA delivery to a variety of tissues remains an obstacle for this technology. To date, siRNA delivery to muscle has only been achieved by local administration or by methods with limited potential use in the clinic. We report systemic delivery of a highly chemically modified cholesterol-conjugated siRNA targeting muscle-specific gene myostatin (*Mstn*) to a full range of muscles in mice. Following a single intravenous injection, we observe 85–95% knockdown of Mstn mRNA in skeletal muscle and >65% reduction in circulating Mstn protein sustained for >21 days. This level of Mstn knockdown is also accompanied by a functional effect on skeletal muscle, with animals showing an increase in muscle mass, size, and strength. The cholesterol-conjugated siRNA platform described here could have major implications for treatment of a variety of muscle disorders, including muscular atrophic diseases, muscular dystrophy, and type II diabetes.

Molecular Therapy—Nucleic Acids (2016) **5**, e342; doi:10.1038/mtna.2016.55; published online 2 August 2016
Subject Category: Nucleic acid chemistries siRNAs, shRNAs, and miRNAs

Introduction

RNA-based gene silencing has a wide range of uses, ranging from a target validation tool to therapeutic applications. It provides a strong alternative to pharmacological compounds which often display toxicity and/or off-target effects, and it provides access to genes that were previously considered difficult to drug or "undruggable" by pharmacological agents. Since the gene-silencing mechanism is based on inhibiting expression of a specific gene target, it may provide a safer alternative for the treatment of a diverse selection of genetic and pathological diseases. Two of the most commonly used gene-silencing platforms are short interfering RNAs (siRNAs) and antisense oligonucleotides (ASOs). siRNAs are 21–23 nucleotide long double-stranded RNAs, which through their interaction with an RNA-induced silencing complex, result in RNA-induced silencing complex recruitment, cleavage, and degradation of target mRNA transcripts.[1] In contrast, ASOs are 12–22 nucleotide long single-stranded DNAs, which block target mRNA gene expression through any of several mechanisms, which include activation of RNase H-mediated degradation, interference with mRNA splicing, or steric hindrance of mRNA translation of the target mRNA.[2]

siRNAs are an important tool for gene silencing in cell lines and animal models. In recent years, advances in oligo design and chemical modification types and patterns have resulted in oligos with increased resistance to nuclease-mediated degradation, improved pharmacokinetics, increased gene specificity, and reduced immunostimulatory responses.[3] While some advances have been made and a few studies have been able to show systemic and targeted systemic siRNA delivery *in vivo*, siRNA delivery to the majority of tissues remains a major obstacle. Systemic siRNA delivery has been limited to tissues such as liver, tumor, spleen, and jejunum.[4–7] *In vivo* siRNA delivery has also been achieved via local delivery in the eye, brain, tumor, and muscle, but local delivery can have limited relevance in clinical therapy.[8–12]

ASOs have also demonstrated gene silencing by systemic administration *in vivo*, delivering to tissues such as liver, adipose, kidney, lung, and tumors.[13–16] However, to date, there has been limited success in siRNA or ASO delivery systemically to muscle, with most reports highlighting muscle targeting by local injection.[17–19] Recent studies by Kawakami *et al.* show both local and systemic delivery of an atelocollagen/siRNA complex to muscle in a mouse model of limb-girdle muscular dystrophy 1C (LGMD1C).[20,21] However, systemic delivery reported in that study was achieved by orbital intravenous delivery, which is both technically challenging and highly invasive.[21] In this study, we use a highly-modified cholesterol-conjugated siRNA designed against myostatin (*Mstn*) to demonstrate effective delivery to whole-body muscles by simple tail vein injection in mice. This cholesterol conjugate shows a high potency and sustained effects on mRNA and protein reduction. Myostatin is an inhibitor of skeletal muscle differentiation and growth. During development, it is an inhibitor of myogenesis, while during adulthood its major role is in negatively regulating satellite cell activation and self-renewal. Myostatin is a member of the TGF-β family and acts as a catabolic stimulus through the ActRIIB receptor, to induce SMAD2/3/FOXO/NF-κB signaling and muscle fiber atrophy.[22,23] Myostatin

[1]Department of RNA Therapeutics Discovery Biology, Merck and Co., Inc, West Point, Pennsylvania, USA; [2]Department of In Vivo Pharmacology, Merck and Co., Inc, West Point, Pennsylvania, USA; [3]Department of Applied Mathematics and Modeling- Scientific Informatics, Merck and Co., Inc, Rahway, New Jersey, USA; [4]Department of Genetics and Pharmacogenomics, Merck and Co., Inc, Boston, Massachusetts, USA. Correspondence: Marija Tadin-Strapps, Department of Genetics and Pharmacogenomics, Merck and Co., Inc, 33 Avenue E Louis Pasteur, Boston, Massachusetts, 02115, USA. E-mail: marija_tadin-strapps@merck.com
Keywords: cholesterol conjugate; muscle; myostatin; siRNA; systemic delivery
Received 8 March 2016; accepted 13 June 2016; published online 2 August 2016. doi:10.1038/mtna.2016.55

deficiency in mice, other animals, and humans is associated with increased muscle mass and strength.[24–26] Attenuation/reversal of muscle atrophy by myostatin deficiency or inhibition has also been demonstrated in different mouse models of muscular dystrophy.[27–30] In addition to effects on mRNA knockdown, the myostatin cholesterol-conjugate used in the current study shows substantial effects on muscle mass and performance in mice. In the future, this class of siRNAs conjugates may have numerous therapeutic applications in a multitude of existing muscle disorders ranging from muscular dystrophy, muscular atrophy in cachexia-inducing diseases, such as cancer, heart disease, chronic obstructive pulmonary disease, sarcopenia, chronic kidney disease, metabolic diseases, and insulin-resistant disorders.[31–34]

Results

Identification of potent Mstn siRNAs in an *in vitro* luciferase assay

A total of 84 unique siRNAs targeting mouse Mstn mRNA sequence were screened in a luciferase reporter assay in Hepa1-6 cells (**Figure 1**). Fourteen siRNAs were selected for further characterization. Based on target mRNA knockdown efficacy and IC_{50} values four siRNAs, all showing a minimum of 90% Mstn mRNA knockdown and IC_{50} values < 1 nmol/l (**Table 1**), were selected for testing *in vivo*.

In vivo screen of Mstn cholesterol-conjugated siRNAs

In vivo efficacy studies in CD-1 mice were performed using the four lead Mstn cholesterol conjugates. Mice were injected intravenously with 15 mpk (mg/kg) siRNA. Only Mstn:(1169)-chol caused a significant reduction in Mstn expression, demonstrating an average of 75% reduction in Mstn mRNA in the gastrocnemius muscle and 50% reduction in circulating protein levels at 72 hours postdose (**Figure 2a**,**b**). This siRNA was selected for use in all follow-up siRNA optimization and functional studies.

Mstn siRNA cholesterol conjugate shows dose-dependent and sustained knockdown of Mstn mRNA in muscle and in circulating protein levels

The Mstn:(1169)-chol siRNA was tested at a range of single doses in mice (5, 15, or 50 mpk) and Mstn mRNA and circulating protein levels were measured at various time points (**Figure 3**). Mstn:(1169)- chol treatment caused a dose-dependent reduction in Mstn mRNA levels in gastrocnemius and triceps muscles (mixed fiber type muscles) and extensor digitorum longus (EDL, a predominantly type II fiber muscle) (**Figs. 3a**-c), demonstrating greater than 8-fold difference in mRNA reduction between the 5 and 50 mpk doses. Significant mRNA reduction was seen at all tested doses with maximum mRNA reduction observed with the 50 mpk dose at day 7, showing 90–95% mRNA knockdown in all three muscles examined (**Figure 3a**–**c**) and 75% reduction in circulating protein levels (**Figure 3d**). The Mstn siRNA also displayed an impressive duration of silencing, maintaining 90–95% mRNA reduction and 65% serum protein reduction for 21 days after 50 mpk dosing. There was no evidence of liver toxicity or muscle damage at all doses examined, as determined by monitoring serum alanine transaminase (ALT)/aspartate transaminase (AST) and muscle creatine phosphokinase, respectively (data not shown).

Mstn mRNA knockdown was comparable between muscles of the hindlimb, forelimb, and back (data not shown), as well as in different fiber type muscles (**Figure 3a**–**c**). Mstn mRNA knockdown effects could not be determined in the soleus muscle due to low Mstn mRNA levels in this muscle (data not shown).

Prolonged Mstn knockdown increases muscle size and alters muscle fatigue profile

Since Mstn is known to have a major inhibitory role in muscle growth, we examined the effects of Mstn silencing by siRNA on muscle mass and function. In order to achieve high levels of Mstn reduction, mice were treated with a single intravenous 50 mpk dose of Mstn-chol siRNA. As shown in

Table 1 Maximum mRNA knockdown and IC50 values of lead Mstn siRNAs as determined from an *in vitro* dose response luciferase reporter assay in Hepa1-6 cells

siRNA	Max mRNA KD (%)	IC_{50} (nmol/l)
Mstn: (1167)	91	0.007
Mstn: (1169)	90	0.005
Mstn: (255)	94	0.004
Mstn: (421)	95	0.016

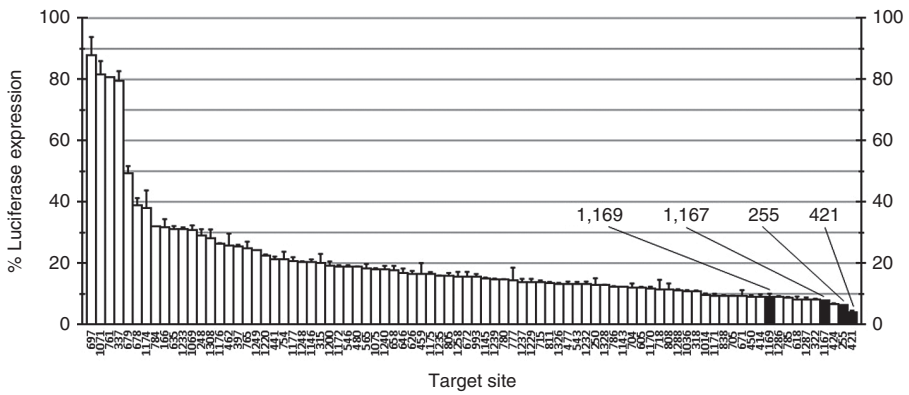

Figure 1 ***In vitro*** **screening of Mstn siRNA sequences.** siRNA screen of 84 Mstn siRNAs in a luciferase reporter assay in Hepa1-6 cells with Lipofectamine 2000. Mstn siRNAs (10 nmol/l), along with Mstn luciferase reporter plasmid (0.6 ng/μl) were cotransfected into cells and luciferase reporter activity was measured after 48 hours post-transfection as a reflection of mRNA knockdown. The four lead siRNAs selected for testing in follow-up *in vivo* screens are indicated by black bars. Bars represent the mean of two biological replicas ± SD.

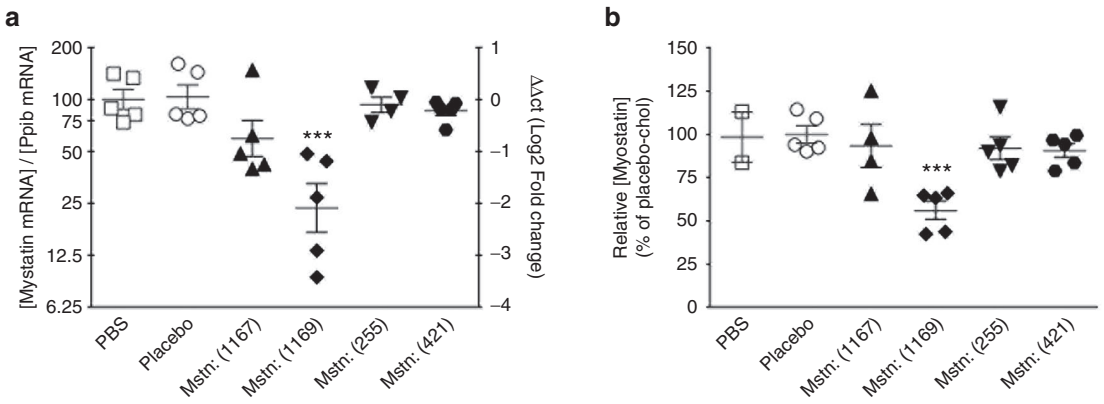

Figure 2 ***In vivo*** **screen of Mstn-chol conjugates**. Four Mstn-chol siRNAs (filled shapes), PBS (□), and Placebo-chol non-targeting control (o) were screened in CD-1 mice ($n = 5$/group) at a 15 mpk dose by i.v. injection. (**a**) Mstn mRNA expression was determined based on ΔΔCt calculations, relative to PBS, in gastrocnemius muscle 3 days postinjection. (**b**) Mstn protein levels were measured in serum 3 days after dosing. ***$P < 0.001$ (by one-way analysis of variance).

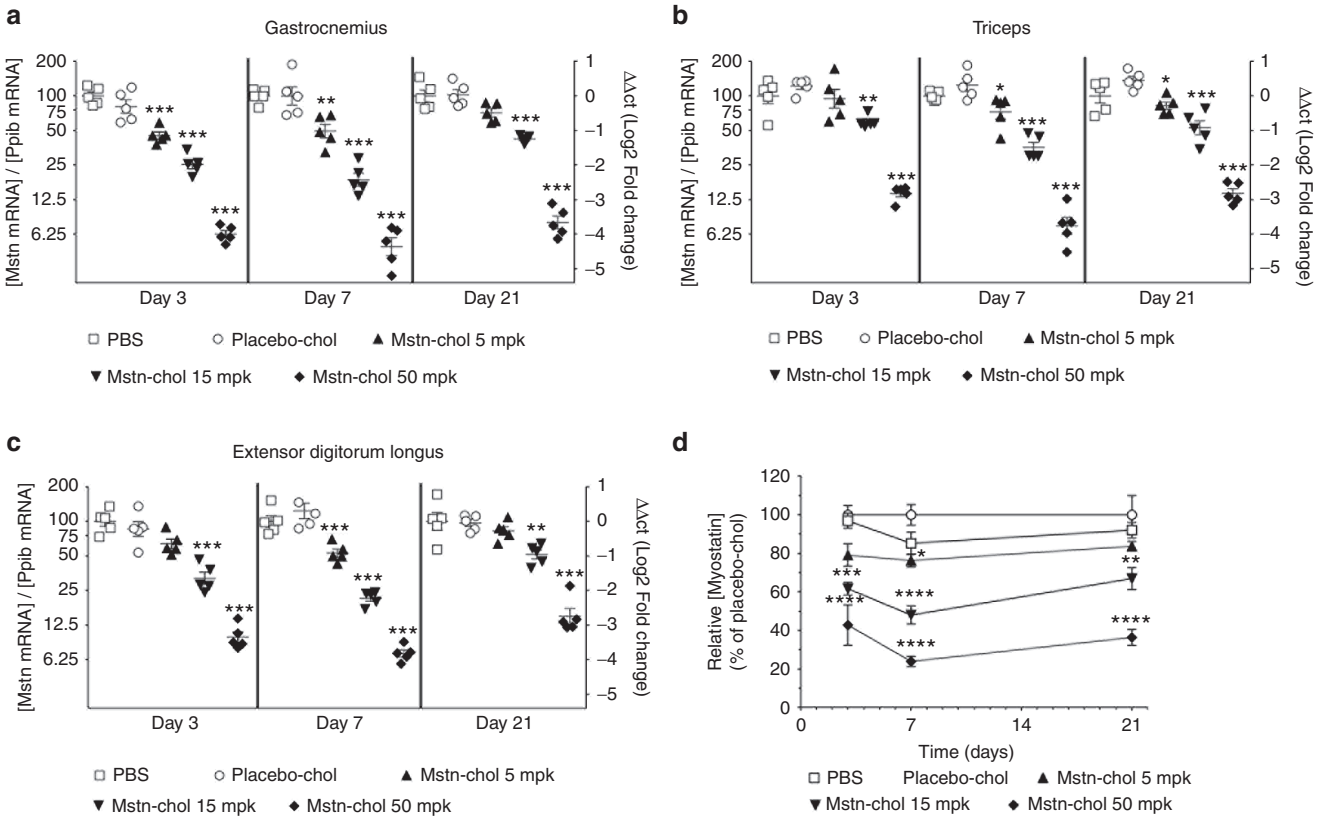

Figure 3 ***In vivo*** **dose titration and duration of Mstn mRNA knockdown by lead Mstn-chol siRNA**. Mstn: (1169) siRNA was tested in CD-1 mice ($n = 5$/group) at 5, 15, and 50 mpk (filled shapes), in addition to PBS (□) and Placebo nontargeting control (o) (50 mpk) by i.v. injection (**a–c**) Mstn mRNA expression was determined based on ΔΔCt calculations, relative to PBS, in gastrocnemius, extensor digitorum longus (EDL), and triceps muscles at day 3, 7, and 21 postinjection. (**d**) Serum Mstn protein levels were measured at indicated timepoints. All statistical analyses were performed relative to Placebo-chol. *$P < 0.05$, **$P < 0.01$, ***$P < 0.001$ (by one-way analysis of variance).

Figure 4a, both phosphate-buffered saline (PBS) and Placebo-chol treatments were used as controls for Mstn-chol treatment, but for simplicity only Placebo-chol data is shown on the subsequent graphs. After 21 days, mice treated with Mstn-chol showed 85–90% reduction in Mstn mRNA in multiple muscles (Figure 4a) and circulating levels of Mstn protein showed >65% reduction for 21 days (Figure 4b). There is a relationship between the reduction of mRNA in muscles and reduction in the level of circulating Mstn protein (Figure 4c). Muscle size was monitored in both hindlimbs of mice by micro-CT at 3, 7, 14, and 20 days after dosing. Maximum muscle cross-sectional area (CSA) for each leg, was determined and indicates a significant increase in muscle size after Mstn-chol treatment as early as 3 days after initiation

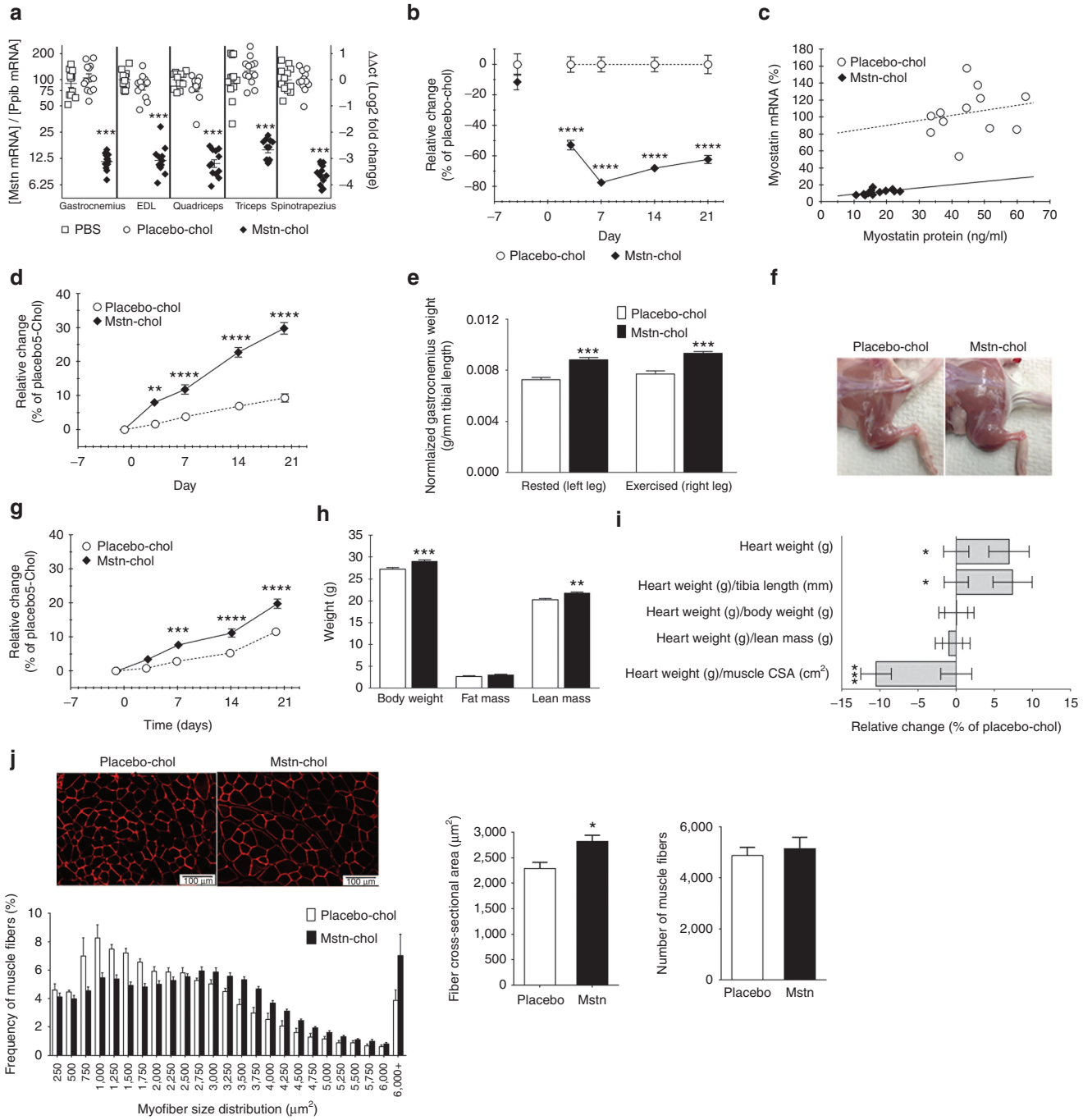

Figure 4 Long-term Myostatin knockdown leads to an increase in muscle size. Mstn (1169) siRNA (◆) and Placebo nontargeting control (o) were dosed intravenously at 50 mpk into CD-1 mice ($n = 12$/group). (**a**) Mstn mRNA levels were determined based on ΔΔCt calculations, relative to PBS, in gastrocnemius, EDL, quadriceps, triceps, and spinotrapezius muscles at day 21 postinjection. (**b**) Serum Mstn protein levels. (**c**) Correlation graph of Mstn mRNA (average of gastrocnemius, EDL, quadriceps, triceps, and spinotrapezius muscles) and serum protein levels. (**d**) Leg muscle size, relative to day-1 placebo control. Maximum cross-sectional area of each hindlimb was quantitated from a series of 10 micro-CT images using a custom MATLAB and Definiens Developer XD software algorithm. (**e**) Gastrocnemius muscle weight of rested leg and exercised leg at day 21. (**f**) Images of hindlimb at day 21. (**g**) Body weight, relative to day-1 placebo control. (**h**) Body composition analysis by qNMR (EchoMRI) at day 20. (**i**) Heart weight measurements are shown normalized to different parameters and indicate the relative change in the specified parameter by Mstn-chol treatment compared to Placebo-chol. (**j**) Laminin immunofluorescent staining of a cross-section of gastrocnemius muscle. Average fiber cross-sectional area and total number of fibers were quantitated using Definiens software ($n = 12$/group). Quantitation of mean fiber area, size frequency distribution of muscle fibers, and mean fiber number is shown. All statistical analyses were performed relative to Placebo-chol. *$P < 0.05$, **$P < 0.01$, ***$P < 0.001$, ****$P < 0.0001$ (by one-way analysis of variance).

of dosing and up to a 20% increase in leg muscle size by day 21 (**Figure 4d**). This data is supported by gastrocnemius muscle weights at day 21/22, which also show ~20% increase in muscle weight by Mstn-chol treatment, compared to control mice (**Figure 4e**). The increase in muscle size is also supported by visual observation of the mouse at day 21, which demonstrates an increase in the hindlimb and the muscles in the lower back region (**Figure 4f**). Body weight (BW) measurements show a 10% increase by day 20 (**Figure 4g**), which body composition analysis suggests is attributable to the increase in lean mass (**Figure 4h**). Immunofluorescent laminin staining (red) of a cross-section of the gastrocnemius muscle suggests that mice treated with Mstn-chol show a 20% increase in average muscle fiber cross-sectional area, while total fiber number remains unchanged (**Figure 4j**). Cell size distribution analysis also reveals a shift toward an increased frequency of larger myofibers.

In addition to skeletal muscle, Mstn has been reported to be expressed at lower levels in the heart.[35] Quantitative polymerase chain reaction (PCR) analysis indicates very low Mstn mRNA expression in the heart (data not shown), and therefore, mRNA knockdown could not be determined. There are varying reports of potential links between Mstn expression levels and cardiac hypertrophy in rodent Mstn knockout models or in response to Mstn inhibition by small molecule/neutralizing antibodies, with some observing an increase in heart size, while others reporting no change in size.[36–39] In order to access signs of cardiac hypertrophy, hearts were weighed and normalized to a variety of parameters (**Figure 4i**). Although Mstn knockdown results in a significant increase in heart weight, there is no evidence of cardiac hypertrophy when normalized to BW or lean mass.

In order to assess changes in the strength and fiber type composition of skeletal muscle as a result of siRNA-mediated reduction of Mstn, muscle fatigue response to exercise was assayed in an *in situ* muscle function assay where repeated isometric contractions are induced by electrostimulation (**Figure 5b–d**). Skeletal muscle consists of different fiber types exhibiting different contractile properties and differential energy source usage. Changes in muscle performance can be determined by changes in several functional parameters.[40] Briefly, fatigue curves exhibit three stages of muscle fatigue: early fatigue, late fatigue, and a nonfatigable stage (**Figure 5a**). "Early fatigue" is represented by F_{max}-F_0 and is indicative of type IIb fibers, which are strong, fast, fatigue very quickly, and use creatine phosphate as an energy source. This stage is followed by "late fatigue" (F_0-F_{min}), primarily indicative of type IIa/x fibers, which are strong, fast, more fatigue-resistant, and use glycogen as an energy source. The final stage of the fatigue curve is the "non-fatigable" stage (F_{min}), which is marked type I fibers, which are weak, slow, nonfatigable, and use fatty acids as an energy source. Mstn knockdown results in increased F_{max} and F_0, and no significant change in F_{min}. Since F_{max}-F_0 remains unchanged, the "early fatigue" stage is

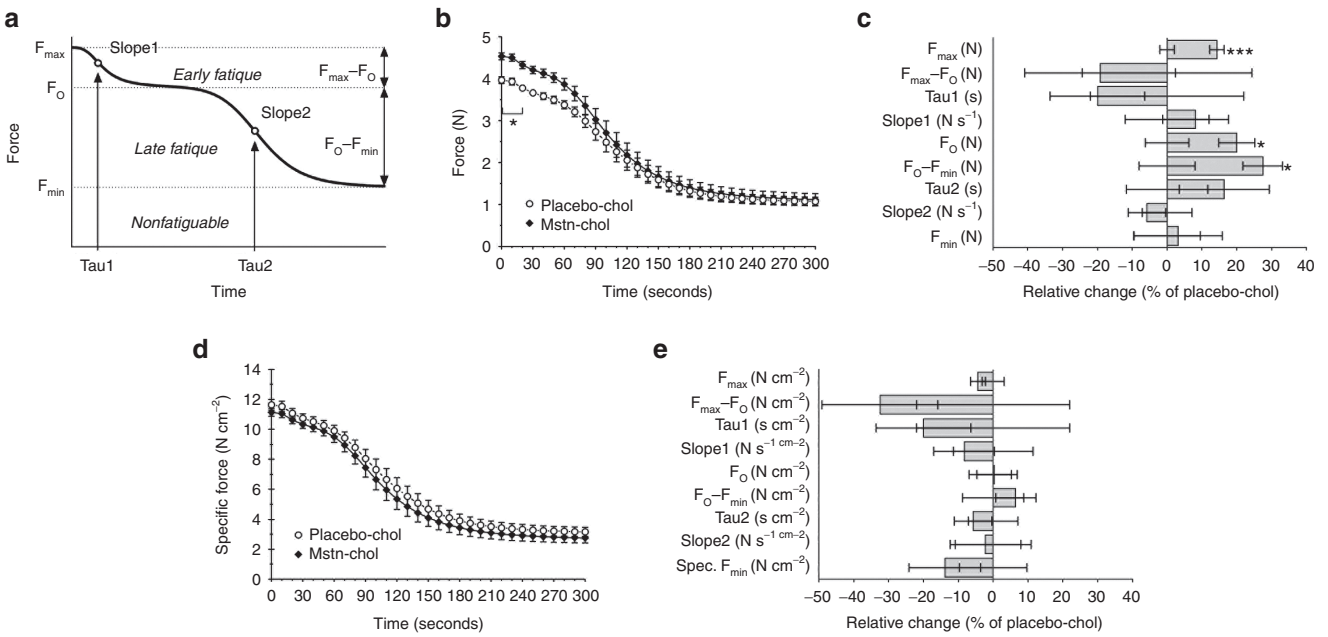

Figure 5 Long-term Myostatin knockdown leads to changes in muscle function. Mstn (1169) siRNA (◆) and Placebo non-targeting control (o) were injected intravenously at 50 mpk into CD-1 mice (n = 12/group). (**a**) Example of a muscle fatigue curve. Fatigue curves exhibit three stages of muscle fatigue: early fatigue, late fatigue, and a nonfatigable stage. "Early fatigue," is represented by F_{max}-F_0, typically representative of type IIb fibers, which use creatine phosphate as an energy source. This stage is followed by "late fatigue" (F_0-F_{min}), typically representative of type IIa/x fibers, which use glycogen as an energy source. The final stage of the fatigue curve is the "non-fatigable" stage (F_{min}), which is indicative of type I fibers, which use fatty acids as an energy source. (**b,d**) Muscle fatigue curves: force (**b**) or specific force (**d**) were generated from an *in situ* muscle function assay performed on the plantar flexor muscle group on day 21 or day 22 (n = 9 total/group). Function parameters calculated from "Force" fatigue curve (**c**) or calculated from "Specific force" fatigue curve (**e**) indicate the relative change in the specified parameter by Mstn-chol treatment compared to Placebo-chol. Statistical analyses for the force curves and the functional parameters derived from these curves were performed using two-way analysis of variance and Bonferroni's multiple comparisons test. *P < 0.05, **P < 0.01, ***P < 0.001.

unaffected (**Figure 5b**,**c**), while the significant increase in F_0-F_{min} suggests an increase in "late fatigue." This data suggests that Mstn knockdown results in a change in type IIa/x fibers, possibly by an increase in the size, quantity, or strength of these fibers. In addition, there is no change in any of the parameters associated with the timing of the fatigue stages (τ_1, τ_2, S_1, S_2), suggesting that fuel availability and usage are unaffected. In order to determine changes to muscle quality, "specific force" was calculated by normalizing absolute force to muscle CSA (**Figure 5d**). There is no significant difference in specific force or any additional functional parameter in response to Mstn knockdown (**Figure 5d**,**e**), suggesting that there is no effect on muscle quality.

Discussion

RNAi-based and ASO-based gene-silencing methodology represents a promising strategy for the inhibition of specific disease pathways. It has the potential to surpass standard pharmacological drugs because of the potential for increased specificity and reduced toxicity and side-effects. Most siRNA and ASO studies in muscle have been constrained to local delivery techniques, such as intramuscular injections, which are not ideal if delivery to multiple muscles is a necessity.[17–19,41]

In recent years, the use of the carrier polymer, atelocollagen, has gained attention for its efficient delivery of nucleic acids (siRNA, ASOs, and plasmids) and negatively-charged proteins. Atelocollagen is an efficient carrier of nucleic acids in the liver, various cancer and xenograft models, and inflammatory models.[42–45] siRNA delivery to skeletal muscle has been demonstrated by local or systemic injection of an Mstn siRNA/atelocollagen complex in mouse models of muscular dystrophy and LGMD1C.[21,46] Kinouchi *et al.*, demonstrated delivery to the quadriceps by intravenous injection into the orbital vein, resulting in 25% knockdown in Mstn protein and an increase in muscle mass in mdx mice after 3 weeks.[46] In order to attain efficacy in muscle, multiple dosing was required during this period. Treatment of a LCMD1C mice (a model of limb girdle muscular dystrophy 1C) with the same regimen of Mstn siRNA/atelocollagen complex was also shown to increase lower limb muscle mass and also improved muscle contractile force generation.[21]

In the current study, we report muscle delivery and efficacious gene silencing using a Mstn cholesterol-conjugated siRNA. A single 50 mpk dose by intravenous tail vein injection demonstrates 85–95% mRNA reduction in multiple muscles across different regions of the mouse and >65 % serum protein reduction sustained for 21 days (**Figure 3a**,**b**). Similar levels of Mstn gene silencing were observed in mixed fiber type and type II fiber type muscles (**Figure 3a**). However, due to low expression levels in the soleus muscle, Mstn knockdown in a type I fiber muscle could not be examined. In support of fiber type-independent gene silencing, unpublished data with a cholesterol conjugate targeting a ubiquitously-expressed gene shows similar knockdown levels in soleus (type I), EDL (type II), and gastrocnemius muscles (mixed) (unpublished data).

Quantitative analysis of muscle CSA in the hindlimb by microCT indicates a 20% increase in plantar flexor muscles by Mstn-chol treatment (**Figure 4e**). Muscle fiber size and cell number quantitation suggests that the increase in muscle size is likely due to muscle fiber hypertrophy, not hyperplasia (**Figure 4j**). The 23% increase in average fiber cross-sectional area is consistent with the 20% increase in muscle CSA. Although both muscle hypertrophy and hyperplasia have been observed in Mstn knockout mice, differences between our model and the Mstn knockout model are likely due to the complete absence of myostatin during the entire development of Mstn knockout mice versus having "acute" inhibition of Mstn in adult animals for siRNA targeting.[47] Our data is consistent with other short-term myostatin inhibition or gene knockdown studies, which also detect only increased muscle hypertrophy.[39] As a result of prolonged Mstn reduction in a wide range of muscles, there is also evidence of changes in muscle performance, as evident in muscle fatigue curves generated from the *in situ* muscle function assay (**Figure 5b**). After 21 days of Mstn knockdown, mice exhibited increased contractile force in the late fatigue stage, indicative of changes affecting type IIa/x fibers (**Figure 5b**, upper). Similarly, improvements in muscle strength have also been reported by other groups in Mstn inhibition studies, which show that mice treated with Mstn neutralizing antibodies for 8 weeks displayed increased grip strength.[39,48]

Studies also suggest that Mstn could have a potential role in regulating heart growth. However, there are conflicting reports, with some observations of cardiac hypertrophy in genetic Mstn knockout mouse models and other preclinical disease models (genetic knockout, neutralizing antibodies, and inhibitors), whereas others report no effect on heart size.[36–39] A study by Artaza, *et al.* finds a 24% increase in heart weight in Mstn knockout mice, but no overall effect on cardiac function.[37] Similarly, Rodgers, *et al.* also reports an increase in absolute heart size by echocardiography measurements in Mstn knockout but no change in heart weight when normalized to body weight.[36] Extensive echocardiographic analysis reveals that the increase in heart weight was associated with improvements in cardiac function, suggesting physiological not pathological hypertrophy. The cardiac profile of Mstn knockout mice exhibits reduced systolic contraction functions at rest and an exaggerated β-adrenergic response. After 21 days of Mstn reduction, we find an increase in absolute heart weight, but not when normalized to BW or lean mass (**Figure 4g**). Our data suggest that Mstn knockdown results in physiological cardiac hypertrophy and is likely a direct reflection of the increase in body weight, acting as a compensatory mechanism, rather than pathological cardiac hypertrophy.

Cholesterol-conjugated siRNAs have been used in several additional *in vivo* studies to demonstrate uptake into liver, small intestine, heart, kidney, adipose, and lung.[6,49–51] To date, there are no reports of chol-siRNA delivery to muscle by systemic administration. Mechanistic studies with our class of cholesterol conjugates in LDL receptor knockout and ApoE knockout mice suggest that mRNA silencing is only partially mediated through the low-density lipoprotein (LDL), very-low-density lipoprotein (VLDL), and intermediate-density lipoprotein (IDL) receptors in liver and muscle (data not shown).

In summary, our study demonstrates the first case of systemic delivery of a siRNA to achieve dramatic and prolonged

gene silencing in muscle leading to effects on muscle function. Several key characteristics of the siRNA make this class of cholesterol conjugate a significant prospect for the future of muscle therapeutics. The Mstn chol-siRNA used in the current study is a simple conjugate that can be intravenously injected, eliminating the requirement for complex formulations or a technically challenging delivery system. The cholesterol conjugate can achieve not only delivery to, but also gene silencing in, skeletal muscles. It exhibits a long duration of silencing from a single dose and appears well-tolerated at high doses. These cholesterol conjugates represent a valuable tool for *in vivo* target validation studies and in the future may be therapeutically beneficial for treating a wide range of muscular dystrophic and atrophic disorders, as well as additional diseases where muscle plays a key role, such as type II diabetes and obesity.

Materials and methods

siRNA synthesis. The siRNAs used in these studies were synthesized by standard methods. For each oligonucleotide, the two individual, complementary strands of the siRNA were synthesized separately using solid-phase synthesis, then purified separately by ion exchange chromatography. The complementary strands were annealed to form the double-strand siRNA (duplex). The duplex was then ultrafiltered and lyophilized to form the solid drug substance. The duplex material was tested for the presence of endotoxin by standard methods. The sequences of lead Mstn siRNAs and the nontargeting control siRNA used in this study are indicated in **Supplementary Table S1** (5′-3′ direction). A single cholesterol moiety was linked to the 3′ end of the passenger strand.

Cells and reagents. Mouse hepatoma Hepa 1–6 cell line was obtained from the American Type Tissue Collection, cat # CRL-1830 (American Type Tissue Collection, Manassas, VA). Cells were grown in Dulbecco's modified Eagle medium, High Glucose with Glutamax (Invitrogen, Carlsbad, CA) adjusted to 1 mmol/l sodium pyruvate (Invitrogen) and supplemented with 10% fetal bovine serum. Streptomycin and penicillin were added to the media at 100 µg/ml and 100 U/ml, respectively. Cells were cultured at 37 °C in the presence of 5% CO_2.

Generation of luciferase reporter constructs. All siRNAs were screened using the psiCHECK2 dual luciferase reporter system. The luciferase reporter plasmids used in this study were derived from psiCHECK2 vector (Promega, Madison, WI). Through *de novo* synthesis the full-length transcript of mouse myostatin (RefSeq NM_010834) was cloned into the XhoI/NotI sites of the vector.

In vitro screening of siRNAs. Hepa1-6 cells were seeded in 96-well plates at a density of 10,000 cells/ well and incubated at 37 °C. After 24 hours, the cells were cotransfected with siRNAs and the MSTN luciferase reporter plasmid using Lipofectamine 2000 reagent (Life Technologies, Carlsbad, CA). Primary screens were performed by cotransfecting siRNAs with the MSTN plasmid at final concentrations of 10 nmol/l and 0.6 ng/µl, respectively. For six-point dose–response curve experiments, the siRNAs were titrated in a fourfold serial dilution starting at 40 nmol/l with the plasmid concentration remaining constant. The cells were incubated at 37 °C and culture medium was replaced with fresh media 24 hours post-transfection. After an additional 24-hour incubation, reporter Renilla luciferase and control firefly luciferase activities were measured using Dual-Glo Luciferase Assay System (Promega). Normalized reporter activity was calculated by dividing Renilla luciferase activity by firefly luciferase activity of the same sample to normalize for variable transfection efficiency.

Animals. Female CD-1 mice were obtained from Charles River and were between 8–9 weeks old at time of study. Mice were maintained on a 12-hour light and dark cycle with *al libitum* access to water and standard chow diet, no. 5001 (LabDiet, St. Louis, MO). Control and experimental cholesterol-conjugated siRNAs were administered to mice by tail vein injection at indicated dosages. All animal studies were conducted at Merck Research Laboratories in an AAALAC-accredited West Point, PA animal facility using protocols approved by the Institutional Animal Care and Use Committee.

Quantitative real-time PCR analysis. Mice were sacrificed and tissues (gastrocnemius, soleus, EDL, triceps, quadriceps, spinotrapezius, and heart muscles) were homogenized in Trizol (Invitrogen), extracted in 1-bromo-2 chloropropane (Acros Organics, Geel, Belgium), and total RNA was isolated using the MagMax RNA isolation method (Ambion, Foster City, CA). RNA (125 ng) was reverse transcribed using the High Capacity cDNA Reverse Transcription kit (Applied Biosystems, Foster City, CA). Taqman qPCR analysis was performed using an ABI 7900 Real-Time PCR System using TaqMan Fast Advanced Master Mix (Applied Biosystems). All Taqman probes and primers were purchased from Applied Biosystems as prevalidated sets: mouse PPIB Assay ID Mm00478295_m1; mouse Mstn Assay ID Mm01254559_m1. Taqman data analysis was performed on an ABI 7900 Real-Time PCR System, as described previously.[52]

Serum analysis of myostatin protein. Blood was collected by tail vein at the specified time points or by terminal cardiac puncture and serum was analyzed for MSTN protein using the GDF-8/Myostatin Quantikine ELISA kit (R&D Systems, Minneapolis, MN). Briefly, serum samples were activated as described in manufacturer protocol, with the exception that the final activated serum sample had an additional 1:2 dilution in calibrator diluent before assaying.

Body composition. Animal body composition was measured by quantitative magnetic resonance spectroscopy using an EchoMRI instrument (Echo Medical Systems, Houston, TX), in order to determine lean/ fat mass. Measurements were made 20 days after initation of siRNA dosing.

Micro-CT imaging and data analysis. Using the LaTheta micro-CT (LaTheta LCT-100A, Aloka, Echo Medical Systems) a stack of 10 slices was scanned between the knee and fibula-tibia junction. Images were analyzed as previously

described[40] to find the largest CSA of whole muscle in the lower leg. Mice were scanned at day -1 with respect to siRNA dosing and also scanned at day 3, 7, 14, and 21 timepoints.

In situ muscle function assay. A custom built *in-situ* assay system, as previously described,[40] was performed 21 days after siRNA dosing. The Achilles tendon of an anesthetized animal was connected to the lever of a combined servomotor/force transducer unit. Electric impulses were delivered via the sciatic nerve to stimulate the muscles of the lower leg (the plantar flexor muscle group) to contract, while the resulting force was recorded. Tetanic stimulation trains of 50 ms length, containing 4 mA square pulses of 0.1 ms duration at 100 Hz, were repeated at a frequency of 0.8 Hz for 300 seconds. A constant baseline tension of 0.1 N was re-established between stimulations. After completion of the *in situ* assay, the hindlimb muscles were collected for weighing and histology.

Several parameters representing the fatigue envelopes were extracted from a double sigmoidal cure fit, including maximum force (F_{max}), intermediate force (F_o), minimum force (F_{min}), early fatigue force (F_{max}-F_o), late fatigue force (F_o-F_{min}), maximal slope of early fatigue (S_1) and late fatigue (S_2) and time constants of early (τ_1) and late fatigue (τ_2) forces.

Measurement of tibia bone lengths. After sacrificing mice, each hindlimb was stored in 70% ethanol overnight. The following day, legs were stripped of muscle and tissue and length was measured using a digital caliper.

Quantitation of myofiber size and number. In order to detect muscle fiber cell size, laminin staining was performed on gastrocnemius muscle 21 days post-siRNA/control treatment. A transverse cross-section was made through the widest region of the gastrocnemius muscle and was fixed in 10% formalin overnight. Muscle was paraffin-embedded and sectioned (5 µm) by standard methods. Sections underwent heat-induced antigen retrieval using EZ-AR 1 citrate buffer (BioGenex, Fremont, CA) at 103°C for 10 minutes using a BioGenex EZ-Retriever Microwave. After PBS washes, sections were incubated at room temperature for 1 hour with a polyclonal Rabbit anti- Laminin antibody at a 1:100 dilution (Abcam, Cambridge, MA). A goat anti-rabbit A555 immunofluorescent secondary antibody was applied after further PBS washes (Invitrogen), and the slides were mounted using ProlongGold with 4′,6-diamidino-2-phenylindole (DAPI) (Invitrogen). Images were captured on a BX-63 Olympus Microscope using a Hamamatsu ORCA-R2 camera and cellSens Dimension 1.7 software (Olympus, Center Valley, PA). Muscle fiber area and total number of fibers were quantitated on the muscle cross-section using Definiens software (Definiens AG, Munich, Germany). Regions out of focus were eliminated from analysis prior to the segmentation of the image. A multiresolution segmentation algorithm was used to extract the muscle fiber and the endomysiums in the remaining muscle section. Fiber area was determined from 12 mice/group, with 1,200–7,000 cell counts/mouse. Mean fiber size and size frequency distribution of muscle fibers were calculated.

Statistical analyses. Error bars indicate standard errors of the mean. Statistical analyses were performed with one-way analysis of variance followed by Dunnett's post-test using Graphpad Prism 5 software (San Diego, CA), unless otherwise indicated. *P*-value of < 0.05 was considered statistically significant. Any deviation from this type of statistical analysis is detailed in the text.

Supplementary material

Table S1. Sequences of Mstn and control siRNAs used in *in vitro* and *in vivo* experiments.

Acknowledgments We would like to thank Duncan Brown for siRNA design, the oligonucleotide synthesis groups and Robert Celano for providing the siRNA oligos. We are grateful to Stephanie Williams, as well as other members of RNA Therapeutics for technical support of the animal harvests. We would also like to acknowledge Nicholas Vitali for supporting the *in situ* muscle function assay and Discovery Clinical Pathology for serum analysis.

1. Bakhtiyari, S, Haghani, K, Basati, G and Karimfar, MH (2013). siRNA therapeutics in the treatment of diseases. *Ther Deliv* **4**: 45–57.
2. Burnett, JC and Rossi, JJ (2012). RNA-based therapeutics: current progress and future prospects. *Chem Biol* **19**: 60–71.
3. Lares, MR, Rossi, JJ and Ouellet, DL (2010). RNAi and small interfering RNAs in human disease therapeutic applications. *Trends Biotechnol* **28**: 570–579.
4. Frank-Kamenetsky, M, Grefhorst, A, Anderson, NN, Racie, TS, Bramlage, B, Akinc, A *et al.* (2008). Therapeutic RNAi targeting PCSK9 acutely lowers plasma cholesterol in rodents and LDL cholesterol in nonhuman primates. *Proc Natl Acad Sci USA* **105**: 11915–11920.
5. Khoury, M, Louis-Plence, P, Escriou, V, Noel, D, Largeau, C, Cantos, C *et al.* (2006). Efficient new cationic liposome formulation for systemic delivery of small interfering RNA silencing tumor necrosis factor alpha in experimental arthritis. *Arthritis Rheum* **54**: 1867–1877.
6. Wolfrum, C, Shi, S, Jayaprakash, KN, Jayaraman, M, Wang, G, Pandey, RK *et al.* (2007). Mechanisms and optimization of *in vivo* delivery of lipophilic siRNAs. *Nat Biotechnol* **25**: 1149–1157.
7. Schiffelers, RM, Ansari, A, Xu, J, Zhou, Q, Tang, Q, Storm, G *et al.* (2004). Cancer siRNA therapy by tumor selective delivery with ligand-targeted sterically stabilized nanoparticle. *Nucleic Acids Res* **32**: e149.
8. Reich, SJ, Fosnot, J, Kuroki, A, Tang, W, Yang, X, Maguire, AM *et al.* (2003). Small interfering RNA (siRNA) targeting VEGF effectively inhibits ocular neovascularization in a mouse model. *Mol Vis* **9**: 210–216.
9. Zhang, X, Shan, P, Jiang, D, Noble, PW, Abraham, NG, Kappas, A *et al.* (2004). Small interfering RNA targeting heme oxygenase-1 enhances ischemia-reperfusion-induced lung apoptosis. *J Biol Chem* **279**: 10677–10684.
10. Tan, PH, Yang, LC, Shih, HC, Lan, KC and Cheng, JT (2005). Gene knockdown with intrathecal siRNA of NMDA receptor NR2B subunit reduces formalin-induced nociception in the rat. *Gene Ther* **12**: 59–66.
11. Liang, Y, Gao, H, Lin, SY, Goss, JA, Brunicardi, FC and Li, K (2010). siRNA-based targeting of cyclin E overexpression inhibits breast cancer cell growth and suppresses tumor development in breast cancer mouse model. *PLoS One* **5**: e12860.
12. Golzio, M, Mazzolini, L, Moller, P, Rols, MP and Teissié, J (2005). Inhibition of gene expression in mice muscle by *in vivo* electrically mediated siRNA delivery. *Gene Ther* **12**: 246–251.
13. Watts, LM, Manchem, VP, Leedom, TA, Rivard, AL, McKay, RA, Bao, D *et al.* (2005). Reduction of hepatic and adipose tissue glucocorticoid receptor expression with antisense oligonucleotides improves hyperglycemia and hyperlipidemia in diabetic rodents without causing systemic glucocorticoid antagonism. *Diabetes* **54**: 1846–1853.
14. Zanardi, TA, Han, SC, Jeong, EJ, Rime, S, Yu, RZ, Chakravarty, K *et al.* (2012). Pharmacodynamics and subchronic toxicity in mice and monkeys of ISIS 388626, a second-generation antisense oligonucleotide that targets human sodium glucose cotransporter 2. *J Pharmacol Exp Ther* **343**: 489–496.
15. Trembley, JH, Unger, GM, Tobolt, DK, Korman, VL, Wang, G, Ahmad, KA *et al.* (2011). Systemic administration of antisense oligonucleotides simultaneously targeting CK2α and α' subunits reduces orthotopic xenograft prostate tumors in mice. *Mol Cell Biochem* **356**: 21–35.
16. Karras, JG, McGraw, K, McKay, RA, Cooper, SR, Lerner, D, Lu, T *et al.* (2000). Inhibition of antigen-induced eosinophilia and late phase airway hyperresponsiveness by an IL-5 antisense oligonucleotide in mouse models of asthma. *J Immunol* **164**: 5409–5415.
17. Laws, N, Cornford-Nairn, RA, Irwin, N, Johnsen, R, Fletcher, S, Wilton, SD *et al.* (2008). Long-term administration of antisense oligonucleotides into the paraspinal muscles of mdx mice reduces kyphosis. *J Appl Physiol (1985)* **105**: 662–668.

18. Gebski, BL, Mann, CJ, Fletcher, S and Wilton, SD (2003). Morpholino antisense oligonucleotide induced dystrophin exon 23 skipping in mdx mouse muscle. *Hum Mol Genet* **12**: 1801–1811.
19. Hagstrom, JE, Hegge, J, Zhang, G, Noble, M, Budker, V, Lewis, DL *et al.* (2004). A facile nonviral method for delivering genes and siRNAs to skeletal muscle of mammalian limbs. *Mol Ther* **10**: 386–398.
20. Kawakami, E, Kawai, N, Kinouchi, N, Mori, H, Ohsawa, Y, Ishimaru, N *et al.* (2013). Local applications of myostatin-siRNA with atelocollagen increase skeletal muscle mass and recovery of muscle function. *PLoS One* **8**: e64719.
21. Kawakami, E, Kinouchi, N, Adachi, T, Ohsawa, Y, Ishimaru, N, Ohuchi, H *et al.* (2011). Atelocollagen-mediated systemic administration of myostatin-targeting siRNA improves muscular atrophy in caveolin-3-deficient mice. *Dev Growth Differ* **53**: 48–54.
22. Sartori, R, Milan, G, Patron, M, Mammucari, C, Blaauw, B, Abraham, R *et al.* (2009). Smad2 and 3 transcription factors control muscle mass in adulthood. *Am J Physiol Cell Physiol* **296**: C1248–C1257.
23. Stitt, TN, Drujan, D, Clarke, BA, Panaro, F, Timofeyva, Y, Kline, WO *et al.* (2004). The IGF-1/PI3K/Akt pathway prevents expression of muscle atrophy-induced ubiquitin ligases by inhibiting FOXO transcription factors. *Mol Cell* **14**: 395–403.
24. Lin, J, Arnold, HB, Della-Fera, MA, Azain, MJ, Hartzell, DL and Baile, CA (2002). Myostatin knockout in mice increases myogenesis and decreases adipogenesis. *Biochem Biophys Res Commun* **291**: 701–706.
25. Schuelke, M, Wagner, KR, Stolz, LE, Hübner, C, Riebel, T, Kömen, W *et al.* (2004). Myostatin mutation associated with gross muscle hypertrophy in a child. *N Engl J Med* **350**: 2682–2688.
26. McPherron, AC and Lee, SJ (1997). Double muscling in cattle due to mutations in the myostatin gene. *Proc Natl Acad Sci USA* **94**: 12457–12461.
27. Zhou, X, Wang, JL, Lu, J, Song, Y, Kwak, KS, Jiao, Q *et al.* (2010). Reversal of cancer cachexia and muscle wasting by ActRIIB antagonism leads to prolonged survival. *Cell* **142**: 531–543.
28. Chiu, CS, Peekhaus, N, Weber, H, Adamski, S, Murray, EM, Zhang, HZ *et al.* (2013). Increased muscle force production and bone mineral density in ActRIIB-Fc-treated mature rodents. *J Gerontol A Biol Sci Med Sci* **68**: 1181–1192.
29. Heineke, J, Auger-Messier, M, Xu, J, Sargent, M, York, A, Welle, S *et al.* (2010). Genetic deletion of myostatin from the heart prevents skeletal muscle atrophy in heart failure. *Circulation* **121**: 419–425.
30. Zhang, L, Rajan, V, Lin, E, Hu, Z, Han, HQ, Zhou, X *et al.* (2011). Pharmacological inhibition of myostatin suppresses systemic inflammation and muscle atrophy in mice with chronic kidney disease. *FASEB J* **25**: 1653–1663.
31. Rüegg, MA and Glass, DJ (2011). Molecular mechanisms and treatment options for muscle wasting diseases. *Annu Rev Pharmacol Toxicol* **51**: 373–395.
32. Engelen, MP, Schols, AM, Baken, WC, Wesseling, GJ and Wouters, EF (1994). Nutritional depletion in relation to respiratory and peripheral skeletal muscle function in out-patients with COPD. *Eur Respir J* **7**: 1793–1797.
33. Bailey, JL, Zheng, B, Hu, Z, Price, SR and Mitch, WE (2006). Chronic kidney disease causes defects in signaling through the insulin receptor substrate/phosphatidylinositol 3-kinase/Akt pathway: implications for muscle atrophy. *J Am Soc Nephrol* **17**: 1388–1394.
34. Asp, ML, Tian, M, Wendel, AA and Belury, MA (2010). Evidence for the contribution of insulin resistance to the development of cachexia in tumor-bearing mice. *Int J Cancer* **126**: 756–763.
35. Sharma, M, Kambadur, R, Matthews, KG, Somers, WG, Devlin, GP, Conaglen, JV *et al.* (1999). Myostatin, a transforming growth factor-beta superfamily member, is expressed in heart muscle and is upregulated in cardiomyocytes after infarct. *J Cell Physiol* **180**: 1–9.
36. Rodgers, BD, Interlichia, JP, Garikipati, DK, Mamidi, R, Chandra, M, Nelson, OL *et al.* (2009). Myostatin represses physiological hypertrophy of the heart and excitation-contraction coupling. *J Physiol* **587**(Pt 20): 4873–4886.
37. Artaza, JN, Reisz-Porszasz, S, Dow, JS, Kloner, RA, Tsao, J, Bhasin, S *et al.* (2007). Alterations in myostatin expression are associated with changes in cardiac left ventricular mass but not ejection fraction in the mouse. *J Endocrinol* **194**: 63–76.
38. Morissette, MR, Cook, SA, Foo, S, McKoy, G, Ashida, N, Novikov, M *et al.* (2006). Myostatin regulates cardiomyocyte growth through modulation of Akt signaling. *Circ Res* **99**: 15–24.
39. Whittemore, LA, Song, K, Li, X, Aghajanian, J, Davies, M, Girgenrath, S *et al.* (2003). Inhibition of myostatin in adult mice increases skeletal muscle mass and strength. *Biochem Biophys Res Commun* **300**: 965–971.
40. Weber, H, Rauch, A, Adamski, S, Chakravarthy, K, Kulkarni, A, Dogdas, B *et al.* (2012). Automated rodent in situ muscle contraction assay and myofiber organization analysis in sarcopenia animal models. *J Appl Physiol (1985)* **112**: 2087–2098.
41. Tang, Y, Hamed, HA, Poklepovic, A, Dai, Y, Grant, S and Dent, P (2012). Poly(ADP-ribose) polymerase 1 modulates the lethality of CHK1 inhibitors in mammary tumors. *Mol Pharmacol* **82**: 322–332.
42. Honma, K, Iwao-Koizumi, K, Takeshita, F, Yamamoto, Y, Yoshida, T, Nishio, K *et al.* (2008). RPN2 gene confers docetaxel resistance in breast cancer. *Nat Med* **14**: 939–948.
43. Nakazawa, K, Nemoto, T, Hata, T, Seyama, Y, Nagahara, S, Sano, A *et al.* (2007). Single-injection ornithine decarboxylase-directed antisense therapy using atelocollagen to suppress human cancer growth. *Cancer* **109**: 993–1002.
44. Hanai, K, Kurokawa, T, Minakuchi, Y, Maeda, M, Nagahara, S, Miyata, T *et al.* (2004). Potential of atelocollagen-mediated systemic antisense therapeutics for inflammatory disease. *Hum Gene Ther* **15**: 263–272.
45. Kawata, E, Ashihara, E, Kimura, S, Takenaka, K, Sato, K, Tanaka, R *et al.* (2008). Administration of PLK-1 small interfering RNA with atelocollagen prevents the growth of liver metastases of lung cancer. *Mol Cancer Ther* **7**: 2904–2912.
46. Kinouchi, N, Ohsawa, Y, Ishimaru, N, Ohuchi, H, Sunada, Y, Hayashi, Y *et al.* (2008). Atelocollagen-mediated local and systemic applications of myostatin-targeting siRNA increase skeletal muscle mass. *Gene Ther* **15**: 1126–1130.
47. Lee, SJ and McPherron, AC (2001). Regulation of myostatin activity and muscle growth. *Proc Natl Acad Sci USA* **98**: 9306–9311.
48. Mendias, CL, Marcin, JE, Calerdon, DR and Faulkner, JA (2006). Contractile properties of EDL and soleus muscles of myostatin-deficient mice. *J Appl Physiol (1985)* **101**: 898–905.
49. Soutschek, J, Akinc, A, Bramlage, B, Charisse, K, Constien, R, Donoghue, M *et al.* (2004). Therapeutic silencing of an endogenous gene by systemic administration of modified siRNAs. *Nature* **432**: 173–178.
50. Lorenz, C, Hadwiger, P, John, M, Vornlocher, HP and Unverzagt, C (2004). Steroid and lipid conjugates of siRNAs to enhance cellular uptake and gene silencing in liver cells. *Bioorg Med Chem Lett* **14**: 4975–4977.
51. Krützfeldt, J, Rajewsky, N, Braich, R, Rajeev, KG, Tuschl, T, Manoharan, M *et al.* (2005). Silencing of microRNAs *in vivo* with 'antagomirs'. *Nature* **438**: 685–689.
52. Tadin-Strapps, M, Peterson, LB, Cumiskey, AM, Rosa, RL, Mendoza, VH, Castro-Perez, J *et al.* (2011). siRNA-induced liver ApoB knockdown lowers serum LDL-cholesterol in a mouse model with human-like serum lipids. *J Lipid Res* **52**: 1084–1097.

Supplementary Information accompanies this paper on the Molecular Therapy–Nucleic Acids website (http://www.nature.com/mtna)